Molecular SIMS Ionization Probability Studied with Laser Postionization: Influence of the Projectile Cluster
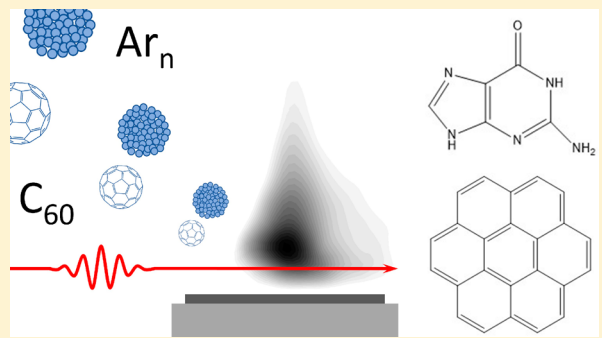
Lars Breuer,*,[†,‡] Hua Tian,[†] Andreas Wucher,[‡] and Nicholas Winograd[†]

[†]The Pennsylvania State University, Department of Chemistry, 104 Chemistry Building, University Park, Pennsylvania 16802, United States

[‡]Fakultät für Physik, Universität Duisburg-Essen, 47048 Duisburg, Germany

S *Supporting Information*

ABSTRACT: The formation probability of (quasi-)molecular secondary ions released from an organic film under bombardment with a 20 keV cluster ion beam is investigated using combined time-of-flight secondary ion and neutral mass spectrometry (ToF-SIMS/SNMS) experiments. The emitted neutral molecules are postionized after their ejection using strong-field photoionization in an intense short infrared laser pulse. Comparing the (quasi-)molecular secondary ion signal with that of the corresponding neutral molecules, the ionization probability of sputtered intact coronene and guanine molecules is determined. The results are compared between two different projectile cluster ions, namely (i) C_{60}^+ and (ii) Ar_n^+ with $n \sim 1000$. It is shown that both projectiles deliver different SNMS spectra, indicating pronounced differences in the collision-induced fragmentation of the emitted molecules. For guanine, the ionization probability obtained with both projectiles is of the same order of magnitude ($\sim 10^{-3}$), with the fullerene cluster producing a slightly larger ionization efficiency than the rare gas cluster. For coronene, on the other hand, a substantially lower ionization efficiency is found for the gas cluster projectile.

INTRODUCTION

Current state-of-the-art approaches to molecular secondary ion mass spectrometry (SIMS) involve the use of cluster projectiles in order to reduce the bombardment-induced fragmentation and damage accumulation at the sample surface.[1−3] Typical primary ions used in that context are either small metal (e.g., Bi_n), fullerene (e.g., C_{60}), or gas (e.g., Ar_n) clusters. Particularly the advent of commercially available gas cluster ion beams (GCIB) delivering projectile ions consisting of up to thousands of atoms or molecules has greatly propelled the field, since it was demonstrated that these projectiles may in some cases allow a nearly fragment-free desorption of intact molecules if optimized in size and impact energy.[4−10] One of the key factors limiting the detection sensitivity in these experiments is the ionization efficiency of the sputtered molecular species,[11−13] and it has been speculated that the low impact energy per cluster constituent required to optimize the fragmentation behavior of a sputtered molecule might also reduce its probability to form a detectable secondary ion.[14] Although many published applications have successfully utilized small, rather unspecific fragment ions to identify certain molecular species in the investigated sample system,[2] it is principally desirable to enhance molecular specificity by detecting (quasi-)molecular ions that represent either the intact parent molecule itself or at least larger molecule specific fragments. The ionization efficiency of such species in the course of the emission event is generally assumed to be rather low,[11] with values down to the

order of 10^{-5} being sometimes quoted in the literature.[15,16] While it is relatively straightforward to measure the useful molecular ion yield, i.e., the number of intact (quasi-)molecular ions detected per molecule equivalent of material removed from a molecular sample, one must realize that this quantity represents a complicated convolution of fragmentation, ionization, and detection probability of a sputtered molecule. In order to judge the prospects for possible sensitivity enhancement via improvements of the ionization efficiency, it is of great interest to unravel these factors and quantitatively determine the ionization probability of the different species ejected from the surface. Ultimately, this task requires the mass-resolved detection of sputtered *neutral* species along with their ionized counterparts, a technique commonly termed secondary neutral mass spectrometry (SNMS).[17] One possible strategy to achieve efficient postionization is to use a pulsed laser beam intersecting the plume of neutral particles emitted from the irradiated surface[18−20] (see refs 21 and 22 for a review). Particularly for sputtered molecular species, single photon absorption[23−26] or strong-field emission[27−29] have been utilized in combination with time-of-flight mass spectrometry as "soft" photoionization methods allowing the detection of sputtered molecules without inducing excessive amounts of photo-

fragmentation. We have recently used strong-field laser postionization (LPI) employing a tightly focused short pulse infrared laser in order to determine a quantitative estimate of the ionization probability for coronene and guanine molecules sputtered under C_{60} cluster ion bombardment.[30,31] In the present work, we expand on these investigations and compare the results obtained with C_{60} projectiles to those obtained with a rare gas cluster ion beam since GCIB are now becoming routinely used in molecular SIMS experiments and have also recently been applied to time-of-flight SNMS techniques.[32]

■ EXPERIMENTAL METHODS

Instrumentation. The time-of-flight (ToF) mass spectrometer used in these experiments has been described in detail elsewhere.[33] In brief, the instrument comprises a 40 keV C_{60}^+ primary ion gun (IOG C60-40, Ionoptika Ltd., Southampton, U.K.),[34] a 20 keV gas cluster ion source (GCIB) (GCIB 20, Ionoptika Ltd., Southampton, U.K.), a controllable temperature sample stage, a reflectron type mass spectrometer, and a microchannel plate (MCP) detector equipped with a high transmission grid above the detector surface and postacceleration capabilities. The two ion beams were aligned to impinge onto the same spot on the investigated sample surface under polar angles of 40° (GCIB) and 45° (C_{60}), respectively, with the azimuth angle between both beams being 135°. Details of the alignment process are given in the Supporting Information. The ToF spectrometer is aligned with its ion optical axis along the sample surface normal and is operated in the delayed extraction mode, where the sample is kept at ground potential during the primary ion pulse and switched to a positive potential of 2500 V afterward, thereby generating a pulsed ion extraction field above the surface. The reflector voltage was set at 6% less than the sample potential, thereby preventing ions starting directly at the surface from being reflected and detected. In connection with the time refocusing properties of the reflectron, this setting determines an effective ion extraction volume located above the surface, henceforth referred to as the *sensitive volume*, from which ions can be extracted and detected as described in detail elsewhere.[21] This volume was then overlapped with a postionizing laser beam running parallel to the sample surface in order to detect sputtered neutral species. For all experiments, the ionization laser and the ion extraction field were fired simultaneously at the end of the primary ion pulse, the width of which was chosen as 5 μs for C_{60}^+ and 25 μs for Ar_n^+ projectile ions. As outlined in the Supporting Information, these settings ensure a velocity-integrated detection of the sputtered particles (secondary ions or postionized neutrals) present in the sensitive volume at the firing time.[21] Mass spectra were acquired in SNMS (laser and primary ion beam active), SIMS (only primary ion beam active), and residual gas background (RGB) (only laser active) mode, and the effective laser postionization (LPI) signal was calculated as the SNMS signal minus both the SIMS and RGB signals. Spectrum acquisition was performed by averaging over 2000−100 000 primary ion pulses with the beam of approximately 60 pA (C_{60}) or 300 pA (GCIB) irradiating an area of about 30−100 μm diameter.

Sample Preparation. Coronene and guanine films were prepared on 10 × 10 mm^2 Si wafers (Ted Pella Inc.) that had been ultrasonicated in chloroform, methanol, and water for 15 min per cycle. The wafers were dried via N_2 stream, attached to the sample block with Cu tape, and introduced to the preparatory chamber of the instrument. An additional chamber was added to the instrument for the purpose of physical vapor

deposition (PVD) of films without exposure to atmosphere. The wafers are cooled by passing N_2 gas through a copper tube submerged in liquid N_2. The cooled gas is then passed through a quartz crystal microbalance (QCM) in contact with the sample block, cooling the block to a temperature of approximately 100 K. An aluminum oxide crucible containing coronene or guanine was heated resistively through a tungsten filament, while the silicon wafers were positioned in the flux of the molecules sublimed from the crucible. Molecular films were deposited to thicknesses of about 200 nm, measured by the QCM.

After the deposition of the film, the cooled sample was transferred from the deposition chamber into the main vacuum chamber and placed in a temperature-controlled sample stage. This sample stage was also cooled by passing N_2 gas through a copper tube submerged in liquid N_2 and afterward through the sample stage. This way the sample was held at approximately 100 K during the experiments.

Laser System. Laser postionization (LPI) of sputtered neutral particles was performed with a commercially available chirped pulse amplification laser system (Coherent Legend Elite Duo, Santa Clara, CA), providing 40 fs pulses of 800 nm radiation at a repetition rate of 1 kHz. The pulses were converted to mid-infrared radiation through an optical parametric amplifier (OPA) (Light Conversion TOPAS-C-HE, Vilnius, Lithuania), with wavelengths tunable from 1160 to 2580 nm. Experiments were performed at 1350 nm with a peak power of about 5×10^{14} W/cm^2 to ionize the sputtered neutral molecules. The laser beam was introduced into the analysis chamber via a CaF_2 window and directed parallel to the sample surface at an azimuth angle of 38° or 175° with respect to the Ar_n^+ or C_{60}^+ primary ion beams, respectively. A 150 mm (at 587.6 nm) BK-7 focusing lens positioned outside the analysis chamber focuses the laser such that the beam waist approximately coincides with the location of the sensitive volume. The lens was translatable in both the horizontal and vertical directions perpendicular to the direction of beam propagation in order to enable a motorized control of the laser focus position above the sample surface. In addition, the lens could be translated in the direction along the laser beam propagation in order to vary the focusing conditions within the sensitive volume. A power meter (Coherent Field Max II TO, Portland, OR) was used to measure the laser power as a 30 s average. The laser intensity in the focal volume was calibrated using xenon gas, which was introduced into the analysis chamber via a controllable leak valve and exhibits a well-known photoionization behavior as a function of the laser intensity.

Experiments investigating the primary ion fluence dependence of the measured signals were performed by alternating between analytical cycles and intermediate ion bombardment cycles, where the analysis was performed either with the pulsed C_{60} or with the pulsed Ar_n^+ beam, while intermediate ion bombardment was always performed with the GCIB operated in dc mode. Spectrum acquisition was performed with the pulsed ion beam rastered across a field of view (FoV) of 100 × 100 μm^2, while the intermediate ion bombardment was carried out rastering the GCIB over a 300 × 300 μm^2 raster area.

At the beginning of each experiment, the laser beam was optimized for maximum LPI signal. As described in detail elsewhere,[35] this procedure involves both the optimum positioning of the laser beam with respect to the plume of sputtered neutral particles and the establishment of optimum focusing conditions, where the laser intensity in the sensitive volume approximately matches the saturation intensity of the neutral molecule under investigation. For the molecules
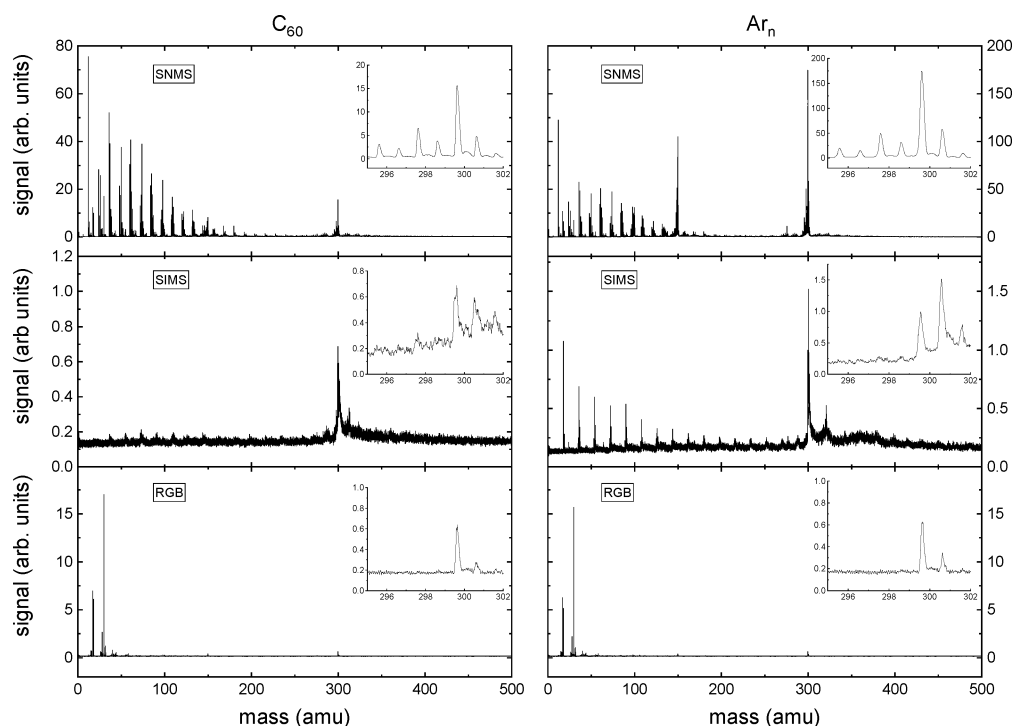
Figure 1. Mass spectra measured for bombardment of a coronene surface with 20 keV C_{60}^+ (left column) and Ar_n^+ cluster projectiles (right column). First row: SNMS spectra measured with the postionization laser placed at optimum position; middle row: SIMS spectra without the postionization laser being fired; bottom row: residual gas background spectra measured with the postionization laser alone.

investigated here, this corresponds to an effective beam diameter of about 200 μm along with a central beam intensity of several 10^{13} W/cm^2. Due to the fact that the laser beam is tightly focused, the effective ionization volume sampled by the postionization experiment is significantly smaller than the extension of the volume from which postionized neutral particles can in principle be extracted and detected. This volume, which is determined by the overlap between the sputtered neutral molecules and the sensitive volume of the TOF spectrometer, has a dimension of the order of millimeters both along and perpendicular to the ion extraction axis (see below). The laser beam diameter is significantly smaller, so that the experiment largely undersamples the detectable LPI signal if the laser is kept at a fixed position. In order to investigate the magnitude of this effect, the laser focusing lens was translated in 200 μm steps both horizontally and vertically with respect to the sample surface, and SNMS spectra were recorded as a function of the laser beam position until the signal vanished. To account for possible signal loss as the experiment proceeds, for instance due to variations in laser power, the signals were measured at the optimal laser position again at the end of each experiment.

■ RESULTS AND DISCUSSION

The goal of this work is to compare the ionization efficiency of sputtered molecules induced by different projectile clusters. In that context, we define the ionization probability of a sputtered species X as

$$\alpha_X^{+,-} = \frac{Y_X^{+,-}}{Y_X} = \frac{Y_X^{+,-}}{Y_{X^0} + Y_{X^+} + Y_{X^-}} \tag{1}$$

where Y_X is the partial sputter yield of X regardless of its charge state, while $Y_X^{+,-}$ and Y_{X^0} denote the partial sputter yields of positively and negatively charged secondary ions X^+, X^-, and

neutrals X^0, respectively. The mass spectrometric signals measured for secondary ions and postionized neutrals, on the other hand, reflect the respective sputter yields via

$$S(X^{+,-}) = I_p \cdot Y_X \cdot \alpha_X^{+,-} \cdot \eta_X^{+,-} \tag{2}$$

and

$$S(X^0) = I_p \cdot Y_X \cdot (1 - \alpha_X^+ - \alpha_X^-) \cdot \alpha_X^0 \cdot \eta_X^0 \tag{3}$$

where I_p and α_X^0 denote the primary ion current and the postionization probability for the sputtered neutrals, respectively. The quantity $\eta_X^{+,-}$ describes an instrumental collection and detection factor which—for the case of postionized neutral particles—also includes the overlap between the ionization laser and the detectable plume. If the laser intensity is high enough, the photoionization process is driven into saturation, meaning that the laser samples 100% of all neutral particles within an effective ionization volume determined by the molecule-specific saturation intensity I_{sat}. As described in detail elsewhere,[36] the value of I_{sat} can be determined from experiments with varying laser intensities, and the volume effectively probed by the laser can then be estimated from a simple barrier suppression photoionization model.[21,37] For the comparative experiments performed here, however, its exact value is not needed, since we are probing the same neutral molecules released from the surface under bombardment with different projectile ion beams. As long as both experiments are performed under exactly the same laser postionization conditions, the effective ionization volume will be the same regardless of the projectile ions used to eject the neutral particles.

The remainder of this chapter is organized as follows. First, we analyze the mass spectra obtained with both projectiles and elucidate some significant differences regarding, for instance, the observed molecular fragmentation patterns. Then, we inves-
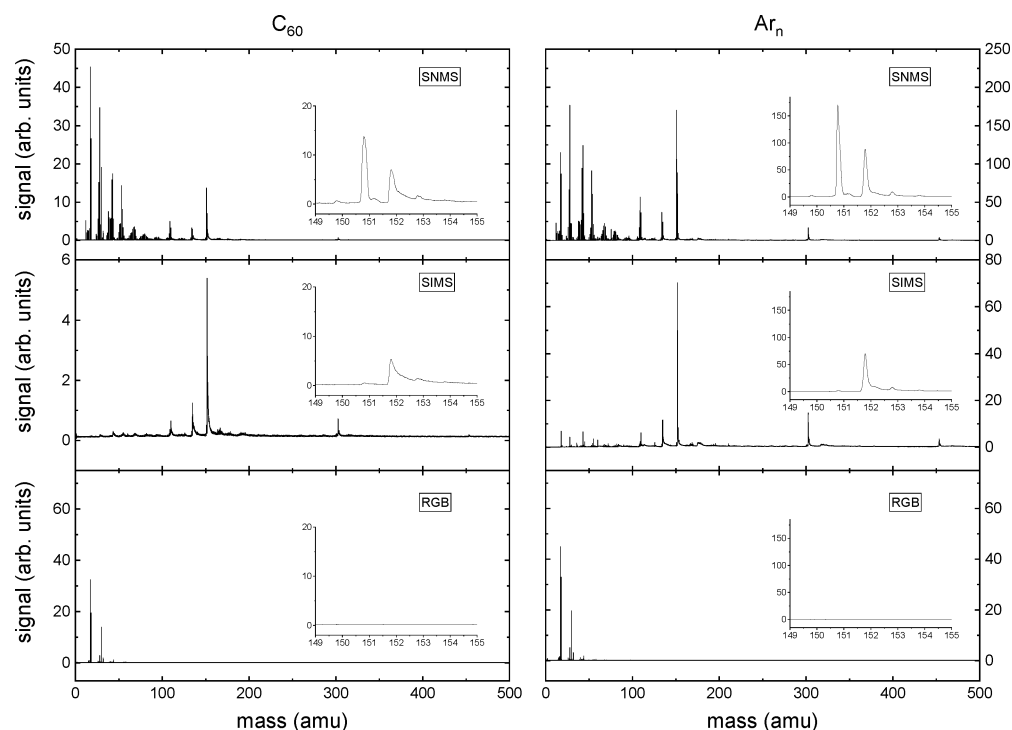
Figure 2. Mass spectra measured for bombardment of a guanine surface with 20 keV C_{60}^{+} (left column) and Ar_n^{+} cluster projectiles (right column). First row: SNMS spectra measured with the postionization laser placed at optimum position; middle row: SIMS spectra without the postionization laser being fired; bottom row: residual gas background spectra measured with the postionization laser alone.

tigate the dependence of the measured ion/neutral ratio on the primary ion fluence in order to find a steady surface state delivering constant ionization probability. As a third step, we then investigate the sampling efficiency of the postionization laser in order to determine the total signal representing the emitted neutral molecules. This signal is then compared with the respective secondary ion signal to determine possible differences in the ionization probability generated by both projectiles.

Mass Spectra. The spectra of coronene and guanine measured with both projectiles are shown in Figure 1 and Figure 2, respectively. In both cases, the postionization laser was positioned such as to produce optimum LPI signal. Note that this position is not necessarily equivalent for both projectiles (see below). The upper panels display the SNMS spectra which are measured with the ion beam and postionization laser on, while the middle row displays the SIMS spectra measured with the postionization laser switched off. The bottom panels display the residual gas background spectra that are measured with the ionization laser only.

The figures clearly show that in both cases molecular ions at m/z 300 (coronene) and 151 (guanine) generated by postionization of sputtered neutral parent molecules are detected in the SNMS spectra. Particularly for the coronene sample bombarded by gas cluster projectiles, abundant postionization signals are also observed at m/z 150 and m/z 100, which correspond to doubly and triply charged parent molecules. The spectra measured for the guanine sample also show molecular dimer and even trimer signals. In principle, the fragmentation of such multimers may constitute a possible way to form (protonated) molecular ions. Since the signals are small compared to those of single molecules, however, this process seems to play only a minor role, and the signals are therefore disregarded in the remainder of this paper. Comparison with the SIMS spectra reveals a significant difference between both

samples. As seen in the insets, coronene bombarded by C_{60}^{+} ions predominantly forms molecular secondary ions M^{+}, followed by a weaker formation of $[M + H]^{+}$ protonated molecules, while the same sample bombarded with gas cluster ions forms both ions with approximately the same efficiency. Guanine, on the other hand, is predominantly ionized via protonation and detected as $[M + H]^{+}$ secondary ions under irradiation with both projectile beams.

Comparing the different scales, the data presented in Figure 1 immediately show that the SIMS ionization efficiency of coronene molecules is significantly smaller for Ar_n^{+} than for C_{60}^{+} projectiles. Under bombardment with gas cluster ions, the signal of postionized neutral coronene molecules is 2 orders of magnitude higher than the corresponding secondary ion signal, thereby demonstrating the enormous sensitivity enhancement that may in some cases be achievable by the LPI technique. Irradiation with C_{60} generates a comparable secondary ion signal along with a much lower postionization signal, so that the molecular SIMS ionization efficiency must be significantly higher. In pronounced contrast, the ratio between $[M + H]^{+}$ secondary ion and M^0 secondary neutral signals measured for *guanine* molecules is comparable in Figure 2, indicating similar SIMS ionization efficiency of these molecules under bombardment with both projectiles. The residual gas background is negligible for guanine, while a measurable signal of postionized gas phase coronene molecules is observed. The latter finding is remarkable since all experiments were performed under cold stage conditions. The signal is negligibly small compared to that of postionized sputtered neutral molecules, though, and therefore does not influence the determination of the ionization probability.

Another remarkable difference between the SNMS spectra depicted in Figure 1 and Figure 2 concerns the fragmentation pattern. In both cases, it is evident that the overall weight of

fragment signals as compared to that of the intact postionized molecules is significantly reduced when gas cluster projectiles are used instead of isoenergetic C_{60}. A similar observation was made by Heeger et al.[38] when comparing Bi_3^+ and Ar_n^+ projectiles. These findings corroborate the notion that larger clusters and, hence, less impact energy per projectile atom leads to a softer sputter ejection process.[4,7,39−41] The data do, however, reveal new information regarding the source of the observed fragmentation pattern. A fundamental problem in any molecular postionization experiment is the fact that postionization of neutral fragments released from the surface in the course of the sputtering process cannot unambiguously be distinguished from fragmentation of sputtered intact molecules in the course of the postionization process. Comparison of SNMS spectra acquired with different projectile beams, as depicted in Figure 1 and Figure 2 and used in ref 38, can shed some light on this question because the employed postionization process is exactly the same for both projectiles. The fact that the spectrum measured under GCIB irradiation reveals much less fragmentation therefore indicates that a large part of the measured LPI fragmentation pattern must arise from postionization of neutral fragments induced by the projectile impact rather than laser-induced photofragmentation of sputtered intact molecules. On the other hand, it is in principle possible that differences in the energetics of sputtering lead to the emission of molecules in different excited states, thereby influencing the photofragmentation pattern. Although this possibility cannot be completely ruled out, we expect these effects to be small in the present case. Further studies using different postionization methods would be needed to clarify this point.

Ionization Probability vs Primary Ion Fluence. In order to establish reproducible surface conditions, the investigated films were prebombarded with the GCIB until stable signals were measured. The dependence of selected SNMS and SIMS signals on the accumulated projectile fluence is shown in Figure 3 for coronene and in Figure 4 for guanine, respectively.

It is seen that the molecular signals measured for coronene decrease with increasing projectile fluence, a finding which is often observed in molecular depth profiling and commonly attributed to the accumulation of impact-induced chemical damage. The signals measured for C and OH radicals follow the same trend, with the C^0 signal gradually becoming slightly more intense as compared to the M^0 signal. Analysis of the spectra measured with the laser alone reveals that this signal exclusively arises from sputtered fragments, while the CO^0 signal contains a significant contribution from the residual gas. The ratio between the molecular secondary ion M^+ and the postionized neutral molecules M^0 (where M represents the intact coronene molecule) is found to increase with increasing projectile ion fluence, until it becomes constant at a "critical dose" of about 3×10^{14} ions/cm^2.

The depth profile measured for the guanine sample is shown in Figure 4. In this case, the signals of postionized neutral guanine molecules and dimers *increase* with increasing projectile fluence, while those measured for neutral H, C, and OH radicals remain approximately constant. Again, the OH^0 signal predominantly arises from a residual gas background, while C^0 and H^0 represent bombardment-induced fragment signals originating from the sample. These signals may in principle include contributions from the guanine molecules and/or a residual gas contamination layer. It is interesting to note that they first rise during the initial stage of the depth profile and then decrease again, while the molecular signals continue to increase.
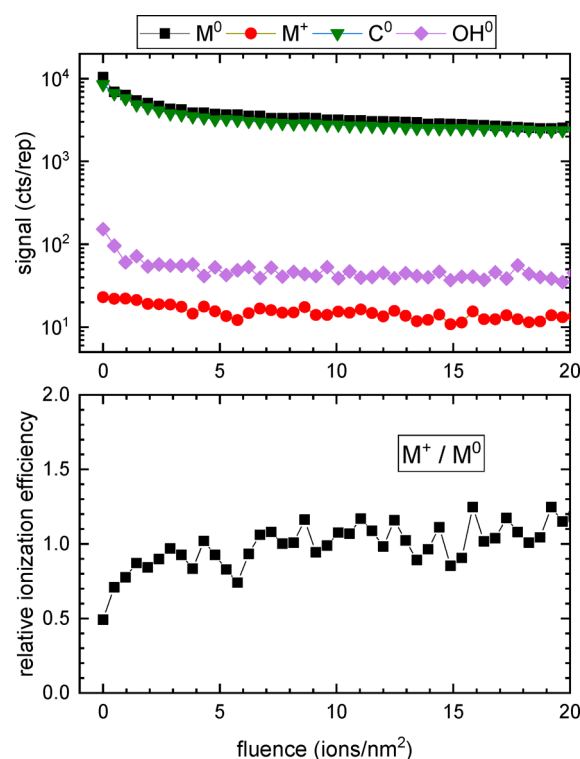

Figure 3. Projectile ion fluence dependence of selected signals (upper panel) and ratio between M^+ secondary ion and M^0 secondary neutral signal (bottom panel) measured for coronene under bombardment with 20 keV Ar_{1000}^+ cluster ions.
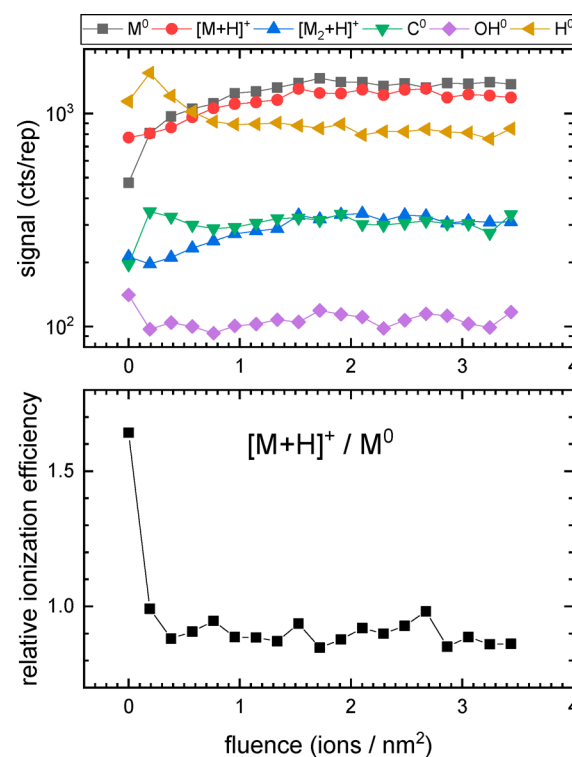

Figure 4. Projectile ion fluence dependence of selected signals (upper panel) and ratio between $[M + H]^+$ secondary ion and M^0 secondary neutral signal (bottom panel) measured for guanine under bombardment with 20 keV Ar_{1000}^+ cluster ions.

Analysis also shows that the molecule dimer is exclusively ejected as a protonated secondary ion, while the guanine monomer is detected as neutral and protonated molecule, respectively. Interestingly, the ratio between the $[M + H]^+$ secondary ion and the postionized neutral M^0 molecule signals initially *decreases* and becomes constant after a relatively small fluence of about 3×10^{13} ions/cm^2. We therefore conclude that a prebombardment of the guanine sample with this fluence would in principle suffice to establish stable conditions for the ionization probability measurement in this case. All molecular signals, however, continue to rise until a fluence of about 2×10^{14} ions/cm^2 is accumulated. Since the secondary ion signals exhibit the same variation as those of the neutral molecules, this rise must reflect an increase of the partial sputter yield of intact guanine molecules. The fact that the prominent fragment signals do not follow this trend indicates that this variation is not due to an increase of the total sputter yield. As a consequence, we are forced to conclude that the surface modification induced by gas cluster bombardment of the guanine surface must act in a way to *enhance* the yield of sputtered neutral guanine molecules against that of the fragments rather than reducing it via accumulated chemical damage. One possible explanation for such a behavior would be that the GCIB sputtering removes a predamaged molecular layer which existed before the depth profile experiment was started. Another possibility would be the removal of a surface contamination layer. In that context, we note again that the investigated samples were produced in a side chamber of the UHV system housing the ToF mass spectrometer, where the molecular films were evaporated onto a precooled silicon substrate and then transferred under UHV conditions to the analysis chamber. The investigated surface was therefore never exposed to air before being analyzed, and the only possible surface modification is by deposition of a thin (water) adsorbate film on the LN2-cooled surface prior to the beginning of the depth profile analysis.

The behavior observed here for guanine is in pronounced contrast to the effect of C$_{60}$ bombardment, which leads to an initial exponential decrease of the molecular signals followed by a slow gradual decrease with increasing fluence.[31] At the same time, the protonation efficiency of a sputtered guanine molecule is increased with increasing C$_{60}$ ion fluence until it becomes constant at about the same critical dose as observed here. We attribute both findings to the chemical damage induced by the C$_{60}$ impact, which acts to decrease molecular sputter yields on one hand and on the other hand may liberate free radicals that help the protonation process.[42] In any case, the depth profile data presented here and in refs 30 and 31 indicate that irradiation of the sample surface with a projectile ion fluence of several 10^{14} ions/cm^2 is sufficient to establish stable conditions regarding the molecular SIMS ionization efficiency, and therefore the experiments discussed in the remainder of this paper were performed after prebombarding the investigated area with the GCIB operated in dc mode and rastered over a surface area of 100×100 μm^2 up to this fluence. The following spectrum acquisition was then performed with the pulsed C$_{60}^+$ or Ar$_n^+$ ion beam operated in spot mode and directed to the center of the preirradiated area.

Photofragmentation. The determination of molecular ionization probabilities via comparison of mass spectrometric signals measured for molecular secondary ions and postionized neutral molecules may in principle be influenced by photofragmentation of the neutral molecules in the ionizing laser beam. More specifically, this may reduce the signal of intact

postionized neutral species, thereby leading to an overestimation of the ionization probability. The influence of photofragmentation on the ionization efficiency measurement as performed here has been extensively discussed in our previous work on C$_{60}^+$ bombardment of coronene[30] and guanine.[31] As described in detail therein, the photofragmentation behavior of a sputtered neutral molecule in the postionization process was investigated by comparing LPI spectra measured for sputtered and thermally evaporated gas phase molecules. As a result, the survival probability of a sputtered molecule was bracketed at values in the range between 5 and 50% for coronene and 8−15% for guanine, thereby permitting to determine upper and lower bounds for the ionization probability.

In the present work, we compare molecular ion signals obtained for the same sputtered molecules under exactly the same postionization conditions. As discussed above, we therefore presume the laser-induced fragmentation of the emitted molecules to be similar regardless of which primary ion is used to initiate the emission process, so that the exact value of the photofragmentation probability is irrelevant in order to compare the secondary ion formation efficiency between both projectiles.

Postionization Efficiency. As explained above, the LPI signal measured with the focused ionization laser adjusted to a single position above the surface severely undersamples the plume of sputtered neutral particles that are in principle detectable by the postionization experiment. The SIMS signal, on the other hand, corresponds to the entire detectable plume of secondary ions that are present above the surface at the time when the extraction field is switched on. A quantitative comparison with the corresponding postionization signal therefore requires to sample the entire detectable plume of neutral particles as well. For that purpose, the laser beam is scanned in directions parallel and perpendicular to the surface, and the resulting LPI signal is summed as described in detail elsewhere.[30,31,35,37]

The resulting scans of the detectable neutral plume are shown in Figure 5 for coronene and Figure 6 for guanine molecules, respectively.

The first observation is that the optimum position of the laser beam is not necessarily the same under irradiation with both projectile ion beams. This finding is understandable since the geometrical shape of the detectable plume depends on the emission angle and velocity distribution of the sputtered neutral particles, which will certainly depend on the projectile nature and impact angle. Since both projectile beams form different azimuth angles with the ionizing laser beam, the differences observed in Figure 5 and Figure 6 are not surprising. The displayed distributions can now be summed to deliver the signal $S_{\text{sum}}^0 = \sum_{i,j} S_{i,j}^0$, which is proportional to the (hypothetical) postionization signal integrated over the entire detectable plume. Relating this signal sum to the signal S_{max}^0 measured with the laser beam set to a fixed laser position such as to deliver maximum signal, we find the apparent sampling efficiency values displayed in Table 1.

In order to determine the true sampling efficiency, these values must be corrected by a factor $v = \pi[R']^2/(\Delta x \cdot \Delta y)$, where Δx and Δy represent the step size used in the laser beam scan and R' denotes the lateral diameter of the effective ionization volume sampled by the laser. Previous LPI investigations of sputtered coronene and guanine molecules have revealed this factor to be of the order of several 10^{-1}.[30,31] Since it constitutes
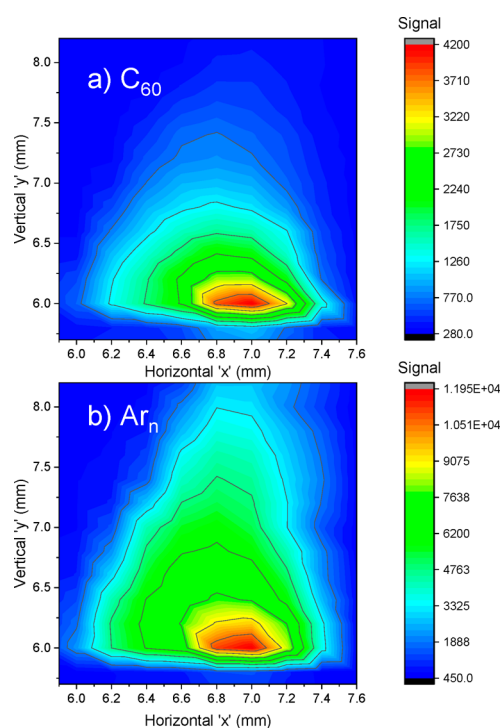
Figure 5. Signal of postionized neutral coronene molecules vs lateral position of the ionizing laser beam for (a) irradiation with 20 keV C_{60}^+ ions and (b) irradiation with 20 keV Ar_n^+ ions.
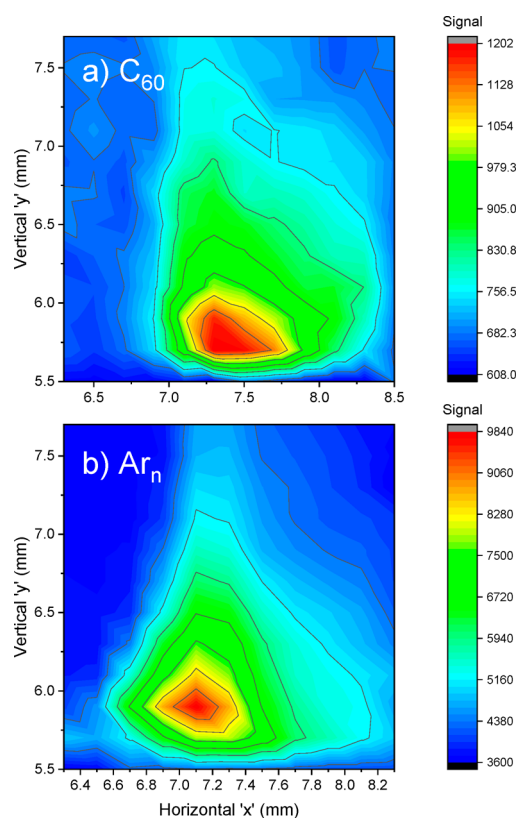

Figure 6. Signal of postionized neutral guanine molecules vs lateral position of the ionizing laser beam for (a) irradiation with 20 keV C_{60}^+ ions and (b) irradiation with 20 keV Ar_n^+ ions.

an instrumental property which—although critically dependent on the laser setup—is independent of the projectile ion beam, its

Table 1. Apparent Sampling Efficiency $S_{max}^0 / \sum S_{i,j}^0$ of the Laser Postionization Experiment with the Ionizing Laser Beam Fixed at the Position Delivering Optimum Signal S_{max}^0 [a]

	C_{60}^+	Ar_n^+
coronene	5.7%	3.5%
guanine	3.0%	3.8%

[a]The error bars of all values are approximately ±0.5%.

exact value is not important for the comparison between different cluster projectiles as targeted here, as long as the postionization conditions remain unchanged when switching between different ion beams. .

Secondary Ion Formation Probability, α^+. The sampling efficiency data displayed in Table 1 can now be used to determine the relative ionization probability of coronene or guanine molecules sputtered by the two different projectile ion beams. For that purpose, the SNMS-, SIMS-, and RGB-spectra displayed in Figure 1 and Figure 2 were integrated over the relevant (quasi-)molecular ion peaks. The SIMS signal was then corrected for the (baseline) background measured without primary ion and laser beam. The true LPI signal of sputtered postionized molecules was evaluated as the SNMS signal summed over all detected charge states minus both the SIMS signal (measured with the primary ion beam on but the laser beam off) and the residual gas signal (measured with the primary ion beam off and the laser beam on). The LPI signal determined this way was then corrected for the relative sampling efficiency displayed in Table 1, and the relative ionization probability was calculated as the ratio between the secondary ion and the corrected postionized neutral signals. The resulting ion/neutral ratios are displayed in Table 2 and Table 3 for sputtered

Table 2. Ratio between Integrated Signals of Molecular Secondary Ions M$^+$ or Protonated Molecules $[M + H]^+$ and Sputtered Neutral Coronene Molecules M^0 Measured for a Coronene Film That Was Prebombarded with the Ar_n^+ Gas Cluster Ion Beam As Described in the Text[a]

	M	$[M + H]$
	M^+/M^0	$[M + H]^+/M^0$
C_{60}	1.3×10^{-3}	4.8×10^{-4}
Ar_n	1.2×10^{-4}	1.3×10^{-4}

[a]The values were calculated by multiplying the signal ratio evaluated from the mass spectra displayed in Figure 1 with the respective relative sampling efficiency depicted in Table 1.

Table 3. Ratio between Integrated Signals of Molecular Secondary Ions M$^+$ or Protonated Molecules $[M + H]^+$ and Sputtered Neutral Guanine Molecules M^0 Measured for a Guanine Film That Was Prebombarded with the Ar_n^+ Gas Cluster Ion Beam As Described in the Text[a]

	M	$[M + H]$
	M^+/M^0	$[M + H]^+/M^0$
C_{60}	1.5×10^{-3}	2.3×10^{-2}
Ar_n	3.0×10^{-4}	1.9×10^{-2}

[a]The values were calculated by multiplying the signal ratio evaluated from the mass spectra displayed in Figure 2 with the respective relative sampling efficiency depicted in Table 1.

coronene and guanine molecules, respectively. While these values correctly reflect the variation of the molecular ionization probability α_M^+ between the two different projectiles, their absolute magnitude is affected by the sampling correction factor ν mentioned above as well as by possible laser-induced fragmentation of the sputtered neutral molecules. It is important to realize, however, that these two influences are exactly the same regardless of the projectile used for sputter desorption and therefore cancel in the determination of the relative ion/neutral ratio.

For coronene, both the secondary ion and neutral spectra were first integrated over the molecular ion peak at m/z 300, delivering the M^+/M^0 values depicted in the first column of Table 2. In addition, both signals were integrated over the peak at m/z 301. For the postionized neutrals, it is found that this peak exclusively reflects the C_{13}-isotope of the coronene molecule M^0, while the secondary ion signal measured at this mass contains contributions from $[M + H]^+$ ions as well as from the C_{13} isotope of the M^+ ion. The $[M + H]^+/M^0$ ratio obtained after correcting the signal for the latter contribution is shown in the second column of Table 2. It is evident that the formation of molecular ions M^+ indeed forms the major ionization channel for coronene molecules released under C_{60} bombardment, but there is also the protonation channel, the efficiency of which is about 37% of that observed for M^+ formation under these irradiation conditions. Under gas cluster impact, on the other hand, both ionization channels occur with similar probability, but the overall ionization efficiency is much smaller than that observed under C_{60} impact. As a central result of this study, we therefore find that the total ionization probability of sputtered coronene molecules via either M^+ or $[M + H]^+$ formation measured under rare gas cluster impact is by approximately 1 order of magnitude smaller than that observed under C_{60} bombardment.

The situation is fundamentally different for sputtered guanine molecules. The results obtained from the evaluation of the spectra shown in Figure 2 are listed in Table 3. In this case, the protonated molecule is detected as the dominant quasi-molecular ion, but there is also a slight possibility for direct molecular ion formation. Interestingly, the M^+ formation probability observed for guanine appears to be larger for the gas cluster than for the C_{60} projectile. The protonation channel, on the other hand, is by more than an order of magnitude more efficient and, in addition, found to be of comparable efficiency for both projectiles. This finding indicates that—at least for the guanine example investigated here—the chemical ionization process leading to $[M + H]^+$ formation does not depend on either the chemical nature of the projectile or the impact energy per cluster atom. In that context, it should be noted that the 20 keV C_{60} and Ar_{1000} cluster projectiles used here correspond to impact energies of 333 and 20 eV per projectile atom, respectively. It has been argued that the ionization efficiency achieved by gas cluster projectiles might drop significantly once the impact energy falls below 10 eV/atom,[14] so that an increase of the gas cluster size might in principle lead to different results than obtained here. Further systematic studies like the one performed here are therefore clearly needed in order to clarify the role of the impact energy on the molecular ionization probability.

A quantitative conversion of the ion/neutral ratio displayed in Table 2 and Table 3 into absolute values of the ionization probability α_M^+ requires knowledge about the effective postionization volume sampled by the laser on one hand and

the influence of laser-induced molecular fragmentation on the other hand. Information regarding the effective postionization volume can be obtained by studying the laser intensity dependence of the measured postionization signals.[30,31,35] This, in turn, requires a careful characterization of the ionizing laser beam which is outside the scope of the present investigation. We note, again, that the exact value of the effective postionization volume is not needed for the study of relative ionization probabilities here since it represents an instrumental quantity which is independent of the projectile used for sputtering. The fragmentation behavior can in principle be investigated by comparing the LPI spectra of sputtered molecules with those obtained for thermally desorbed gas phase molecules. For coronene and guanine, we have recently performed such studies, thereby deriving bracketing values for the survival probability of an intact parent molecule in the course of the sputtering event. As a result, it was found that the M^+ formation probability of a coronene molecule sputtered under 20 keV C_{60} irradiation must reside in the range between 2.5×10^{-4} and 2.5×10^{-3},[30] while the efficiency of $[M + H]^+$ formation from a guanine molecule sputtered under 40 keV C_{60} bombardment was bracketed between 7.5×10^{-4} and 1.5×10^{-3}.[31] In combination with the relative ionization probability data measured here, these values can be used to estimate the molecular ionization efficiency induced by the gas cluster projectiles as $\alpha_M^+ \sim 10^{-5}-10^{-4}$ for coronene and $\alpha_M^+ \sim 10^{-3}$ for guanine, respectively.

■ CONCLUSIONS

Strong field laser postionization of sputtered neutral molecules in combination with time-of-flight mass spectrometry allows to systematically investigate the ionization probability obtained in a molecular SIMS experiment. Using a dual beam setup with two different cluster ion guns pointing at the same irradiated spot at the sample surface, one can utilize the same postionization conditions and directly compare the relative ionization efficiency achieved by different projectile ions by simply switching between the two ion beams. The results obtained for two different molecular films investigated here reveal a fundamentally different ionization behavior for sputtered coronene and guanine molecules.

For the nonpolar coronene molecule, the dominating ionization mechanism is the direct formation of molecular ions, a process which obviously is significantly more efficient under C_{60} than under gas cluster ion bombardment. One possible way to rationalize this finding would be to presume this ionization channel to reflect the transient electronic excitation generated by the projectile impact. Due to the smaller impact energy per atom, the argon gas cluster may be less efficient in that respect, leading to an ionization efficiency which is more than an order of magnitude lower than that observed for C_{60}. For the polar guanine molecule, on the other hand, the dominating ionization channel is the formation of protonated molecules, thereby indicating a chemical rather than a physical ionization process. In fact, the physical ionization efficiency leading to M^+ formation is found to be comparable for both molecules. The chemical ionization mechanism, however, which dominates molecular secondary ion formation for guanine, is practically absent for the coronene molecule. Interestingly, our results show that this ionization mechanism is largely independent of the projectile. Both findings indicate that the chemistry of the sample material determines the efficiency of this ionization mechanism rather than properties of the projectile. Apparently,

both projectiles investigated here must be comparably efficient to generate fragment radicals which are required for $[M + H]^+$ formation. Finally, the finding of a slightly smaller efficiency for the gas cluster coincides with the observation that this projectile generates less neutral fragmentation than the C_{60} projectile.

In discussing these results, one should keep in mind that the relatively small gas cluster investigated here still corresponds to a relatively high impact energy per cluster constituent, where the fragmentation and, hence, radical production might still be quite efficient. On the other hand, systematic studies of secondary ion yields obtained with different clusters indicate that the ionization efficiency of gas clusters may drastically decrease once the impact energy falls below about 10 eV/atom. Further studies like the one performed here are clearly needed in order to clarify this point.

■ ASSOCIATED CONTENT

ⓢ Supporting Information

The Supporting Information is available free of charge on the ACS Publications website at DOI: 10.1021/acs.jpcc.8b10245.

> Measurement of the gas cluster size distribution; timing considerations; ion beam alignment; description of the signal measured in a delayed extraction experiment; measurements on the variation of the sensitive volume (PDF)

■ AUTHOR INFORMATION

Corresponding Author

*E-mail: lars.breuer@uni-due.de.

ORCID ⬤

Lars Breuer: 0000-0002-7797-9662
Hua Tian: 0000-0002-3598-0219

Notes

The authors declare no competing financial interest.

■ REFERENCES

(1) Winograd, N. The Magic of Cluster Sims. *Anal. Chem.* **2005**, *77*, 142A−149A.

(2) Mahoney, C. M. Cluster Secondary Ion Mass Spectrometry of Polymers and Related Materials. *Mass Spectrom. Rev.* **2009**, *29*, 247−293.

(3) *Cluster Secondary Ion Mass Spectrometry: Principles and Applications*; Mahoney, C. M., Ed.; John Wiley & Sons: Hoboken, NJ, 2013.

(4) Matsuo, J.; Ninomiya, S.; Nakata, Y.; Honda, Y.; Ichiki, K.; Seki, T.; Aoki, T. What Size of Cluster Is Most Appropriate for Sims? *Appl. Surf. Sci.* **2008**, *255*, 1235−1238.

(5) Matsuo, J.; Ninomiya, S.; Nakata, Y.; Ichiki, K.; Aoki, T.; Seki, T. Size Effect in Cluster Collision on Solid Surfaces. *Nucl. Instrum. Methods Phys. Res., Sect. B* **2007**, *257*, 627−631.

(6) Nakata, Y.; Ninomiya, S.; Matsuo, J. Secondary Ion Emission from Bio-Molecular Thin Films under Ion Bombardment. *Nucl. Instrum. Methods Phys. Res., Sect. B* **2007**, *256*, 489−492.

(7) Ninomiya, S.; Nakata, Y.; Ichiki, K.; Seki, T.; Aoki, T.; Matsuo, J. Measurements of Secondary Ions Emitted from Organic Compounds Bombarded with Large Gas Cluster Ions. *Nucl. Instrum. Methods Phys. Res., Sect. B* **2007**, *256*, 493−496.

(8) Gnaser, H.; Kusakari, M.; Fujii, M.; Seki, T.; Aoki, T.; Matsuo, J. Secondary Ion Emission from Leucine and Isoleucine under Argon Gas-Cluster Ion Bombardment. *J. Vac. Sci. Technol., B: Nanotechnol. Microelectron.: Mater., Process., Meas., Phenom.* **2016**, *34*, 03H102.

(9) Muecksch, C.; Anders, C.; Gnaser, H.; Urbassek, H. M. Dynamics of L-Phenylalanine Sputtering by Argon Cluster Bombardment. *J. Phys. Chem. C* **2014**, *118*, 7962−7970.

(10) Gnaser, H.; Ichiki, K.; Matsuo, J. Strongly Reduced Fragmentation and Soft Emission Processes in Sputtered Ion Formation from Amino Acid Films under Large Ar_n^+ (N ≤ 2200) Cluster Ion Bombardment. *Rapid Commun. Mass Spectrom.* **2012**, *26*, 1−8.

(11) Vickerman, J. C.; Winograd, N. Sims-a Precursor and Partner to Contemporary Mass Spectrometry. *Int. J. Mass Spectrom.* **2015**, *377*, 568−579.

(12) Vickerman, J.; Winograd, N. Cluster Tof-Sims Imaging and the Characterization of Biological Materials. In *Cluster Secondary Ion Mass Spectrometry*; John Wiley & Sons, Inc.: Hoboken, NJ, 2013; pp 269−312.

(13) Fletcher, J. S.; Lockyer, N. P.; Vickerman, J. C. Developments in Molecular Sims Depth Profiling and 3d Imaging of Biological Systems Using Polyatomic Primary Ions. *Mass Spectrom. Rev.* **2011**, *30*, 142−174.

(14) Rabbani, S.; Barber, A. M.; Fletcher, J. S.; Lockyer, N. P.; Vickerman, J. C. Tof-Sims with Argon Gas Cluster Ion Beams: A Comparison with C(60)(+). *Anal. Chem.* **2011**, *83*, 3793−3800.

(15) Fletcher, J. S.; Vickerman, J. C. A New Sims Paradigm for 2d and 3d Molecular Imaging of Bio-Systems. *Anal. Bioanal. Chem.* **2010**, *396*, 85−104.

(16) Sheraz, S.; Barber, A.; Razo, I. B.; Fletcher, J. S.; Lockyer, N. P.; Vickerman, J. C. Prospect of Increasing Secondary Ion Yields in Tof-Sims Using Water Cluster Primary Ion Beams. *Surf. Interface Anal.* **2014**, *46*, 51−53.

(17) Oechsner, H.; Stumpe, E. Sputtered Neutral Mass Spectrometry (Snms) as a Tool for Chemical Surface Analysis and Depth Profiling. *Appl. Phys.* **1977**, *14*, 43−47.

(18) Becker, C. H.; Gillen, K. T. Surface Analysis by Nonresonant Multiphoton Ionization of Desorbed or Sputtered Species. *Anal. Chem.* **1984**, *56*, 1671−1674.

(19) Gruen, D. M.; Calaway, W. F.; Pellin, M. J.; Young, C. E.; Spiegel, D. R.; Clayton, R. N.; Davis, A. M.; Blum, J. D. Selectivity, Specificity and Sensitivity in the Photoionization of Sputtered Species. *Nucl. Instrum. Methods Phys. Res., Sect. B* **1991**, *58*, 505−511.

(20) Kimock, F. M.; Baxter, J. P.; Pappas, D. L.; Korbin, P. H.; Winograd, N. Solids Analysis Using Energetic Ion Bombardment and Multiphoton Resonance Ionization with Time-of-Flight Detection. *Anal. Chem.* **1984**, *56*, 2782−2791.

(21) Wucher, A. Laser Postionization—Fundamentals. In *Tof-Sims: Materials Analysis by Mass Spectrometry*, 2nd ed.; Vickerman, J. C., Briggs, D., Eds.; IM Publications and SurfaceSpectra: Chichester, U.K., 2013; pp 217−246.

(22) Lockyer, N. P. Laser Postionization for Elemental and Molecular Surface Analysis. In *Tof-Sims: Materials Analysis by Mass Spectrometry*, 2nd ed.; Vickerman, J. C., Briggs, D., Eds.; IM Publications & SurfaceSpectra: Chichester, U.K., 2013.

(23) Schuehle, U.; Pallix, J. B.; Becker, C. H. Sensitive Mass Spectrometry of Molecular Adsorbates by Stimulated Desorption and Single-Photon Ionization. *J. Am. Chem. Soc.* **1988**, *110*, 2323−2324.

(24) Coon, S. R.; Calaway, W. F.; Burnett, J. W.; Pellin, M. J.; Gruen, D. M.; Spiegel, D. R.; White, J. M. Yields and Kinetic Energy Distributions of Sputtered Neutral Copper Clusters. *Surf. Sci.* **1991**, *259*, 275−287.

(25) Wahl, M.; Wucher, A. Vuv Photoionization of Sputtered Neutral Silver Clusters. *Nucl. Instrum. Methods Phys. Res., Sect. B* **1994**, *94*, 36−46.

(26) Lockyer, N. P.; Vickerman, J. C. Single Photon Ionisation Mass Spectrometry Using Laser-Generated Vacuum Ultraviolet Photons. *Laser Chem.* **1997**, *17*, 139−159.

(27) Levis, R. J.; Dewitt, M. J. Photoexcitation, Ionization, and Dissociation of Molecules Using Intense near-Infrared Radiation of Femtosecond Duration. *J. Phys. Chem. A* **1999**, *103*, 6493−6507.

(28) Willingham, D.; Kucher, A.; Winograd, N. Strong-Field Ionization of Sputtered Molecules for Biomolecular Imaging. *Chem. Phys. Lett.* **2009**, *468*, 264−269.

(29) Longobardo, A.; Macpherson, A. N.; Vickerman, J. C.; Lockyer, N. P. New Prospects for Molecular Post-Ionisation Using Femtosecond Ir Lasers. *Surf. Interface Anal.* **2013**, *45*, 525−528.

(30) Popczun, N. J.; Breuer, L.; Wucher, A.; Winograd, N. On the Sims Ionization Probability of Organic Molecules. *J. Am. Soc. Mass Spectrom.* **2017**, *28*, 1182−1191.

(31) Popczun, N. J.; Breuer, L.; Wucher, A.; Winograd, N. Ionization Probability in Molecular Secondary Ion Mass Spectrometry: Protonation Efficiency of Sputtered Guanine Molecules Studied by Laser Postionization. *J. Phys. Chem. C* **2017**, *121*, 8931−8937.

(32) Pelster, A.; Körsgen, M.; Heeger, M.; Arlinghaus, H. F. Implementation and Optimization of Large Gas Cluster Laser Post-Ionization Secondary Neutral Massspectrometry for Molecular Analysis. *J. Phys. Chem. C* **2017**, *121*, 15266−15271.

(33) Braun, R. M.; Blenkinsopp, P.; Mullock, S. J.; Corlett, C.; Willey, K. F.; Vickerman, J. C.; Winograd, N. Performance Characteristics of a Chemical Imaging Time-of-Flight Mass Spectrometer. *Rapid Commun. Mass Spectrom.* **1998**, *12*, 1246−1252.

(34) Weibel, D. E.; Wong, S.; Lockyer, N. P.; Blenkinsopp, P.; Hill, R.; Vickerman, J. C. A C_{60} Primary Ion Beam System for Time of Flight Secondary Ion Mass Spectrometry: Its Development and Secondary Ion Yield Characteristics. *Anal. Chem.* **2003**, *75*, 1754−1764.

(35) Kucher, A.; Wucher, A.; Winograd, N. Strong-Field Ionization of Beta-Estradiol in the Ir: Strategies to Optimize Molecular Postionization in Secondary Neutral Mass Spectrometry. *J. Phys. Chem. C* **2014**, *118*, 25534−25544.

(36) Hankin, S. M.; Villeneuve, D. M.; Corkum, P. B.; Rayner, D. M. Nonlinear Ionization of Organic Molecules in High Intensity Laser Fields. *Phys. Rev. Lett.* **2000**, *84*, 5082−5085.

(37) Breuer, L.; Kucher, A.; Herder, M.; Wucher, A.; Winograd, N. Formation of Neutral In_nc_m Clusters under C_{60} Ion Bombardment of Indium. *J. Phys. Chem. A* **2014**, *118*, 8542.

(38) Heeger, M.; Tyler, B. J.; Körsgen, M.; Arlinghaus, H. F. Laser Postionization of Neutral Molecules Sputtered Using Bismuth and Argon Cluster Primary Ions. *Biointerphases* **2018**, *13*, 03B412.

(39) Kayser, S.; Rading, D.; Moellers, R.; Kollmer, F.; Niehuis, E. Surface Spectrometry Using Large Argon Clusters. *Surf. Interface Anal.* **2013**, *45*, 131−133.

(40) Ninomiya, S.; Ichiki, K.; Seki, T.; Aoki, T.; Matsuo, J. The Emission Process of Secondary Ions from Solids Bombarded with Large Gas Cluster Ions. *Nucl. Instrum. Methods Phys. Res., Sect. B* **2009**, *267*, 2601−2604.

(41) Ninomiya, S.; Nakata, Y.; Honda, Y.; Ichiki, K.; Seki, T.; Aoki, T.; Matsuo, J. A Fragment-Free Ionization Technique for Organic Mass Spectrometry with Large Ar Cluster Ions. *Appl. Surf. Sci.* **2008**, *255*, 1588−1590.

(42) Wucher, A. Molecular Secondary Ion Formation under Cluster Bombardment: A Fundamental Review. *Appl. Surf. Sci.* **2006**, *252*, 6482−6489.